



Berg Huettenmaenn Monatsh (2023) Vol. 168 (3): 130–136

<https://doi.org/10.1007/s00501-023-01326-7>

© The Author(s), under exclusive licence to Austrian Society for Metallurgy of Metals (ASMET) and Bergmännischer Verband Österreich (BVÖ) 2023

BHM Berg- und Hüttenmännische Monatshefte

Plasma Nitriding Properties of Sintered Body Formed Using CoCrFeMnNi High-Entropy Alloy Powder by Varying Ball-Milling Duration

Jiaxin Peng¹ and Akio Nishimoto²¹Graduate School of Science and Engineering, Kansai University, Osaka, Japan²Department of Chemistry and Materials Engineering, Faculty of Chemistry, Materials and Bioengineering, Kansai University, Osaka, Japan

Received January 19, 2023; accepted February 6, 2023; published online March 2, 2023

Abstract: Recently, a CoCrFeMnNi high-entropy alloy (HEA) was reported to possess excellent tensile strength and ductility at low temperatures. By plasma nitriding at 673 K, an expanded face-centered cubic structure was formed on the surface of this HEA. Another study found that, on ball milling, dislocations were introduced on the surface of a CoCrFeMn alloy powder and consequently strength improvement and strain hardening occurred simultaneously. The present study aimed to evaluate the characteristics of the nitrided layer obtained by direct-current plasma nitriding (DCPN) treatment of the sintered body of a CoCrFeMnNi HEA powder formed after ball milling. Specifically, first ball-milling was conducted on gas-atomized CoCrFeMnNi HEA powder samples for durations ranging from 0 to 15 h to prepare sintered bodies. Subsequently, each sintered body was subjected to DCPN treatment at 673 K for 15 h at a gas pressure of 200 Pa under 75% N₂–25% H₂. During the plasma nitriding process, an austenitic stainless-steel screen was installed as an auxiliary cathode to ensure uniform heating and high nitrogen supply. Furthermore, each nitrided sample was characterized by X-ray diffraction (XRD), cross-sectional microstructure observations, surface morphology observations, Vickers hardness tests, glow discharge optical emission spectroscopic analysis (GD-OES), corrosion tests, and wear tests. The XRD and GD-OES results showed that N concentration on the surface decreased with the ball milling duration. Based on the Vickers hardness tests, the surface hardness increased

with the ball milling duration. Electron-probe microanalysis and scanning electron microscopy results exhibited that the deposited and nitrided layers separated on the surfaces of all plasma-nitrided samples. The wear tests showed that the widths and depths of the wear marks decreased with increasing ball milling duration, and thus the samples presented an increased wear resistance.

Keywords: High-entropy alloy, Plasma nitriding, Ball milling, Gas-atomized powder, Nitrided layer, Spark plasma sintering, Surface modification

Plasmanitrierungseigenschaften von Sinterkörpern hergestellt aus dem Pulver einer hochentropischen CoCrFeMnNi-Legierung bei unterschiedlicher Dauer des KugelfräSENS

Zusammenfassung: Kürzlich wurde über eine hochentropische CoCrFeMnNi-Legierung (HEA) berichtet, die eine ausgezeichnete Zugfestigkeit und Duktilität bei niedrigen Temperaturen aufweist. Durch Plasmanitrierung bei 673 K wurde auf der Oberfläche dieser HEA eine erweiterte kubisch-flächenzentrierte Struktur gebildet. In einer anderen Studie wurde festgestellt, dass beim KugelfräSEN Versetzungen in die Oberfläche eines CoCrFeMn-Legierungspulvers eingebracht wurden, was zu einer gleichzeitigen Festigkeitssteigerung und Kaltverfestigung führte. In der vorliegenden Studie sollen die Eigenschaften der Nitrierschicht bewertet werden, die durch Gleichstromplasmanitrierung (DCPN) des Sinterkörpers eines nach dem Kugelmahlen hergestellten CoCrFeMnNi HEA-Pulvers erhalten wurde. Konkret wurden die gaserstäubten CoCrFeMnNi HEA-Pulverproben zunächst für eine Dauer von 0 bis 15 h kugelgemahlen, um Sinterkörper herzustellen. Anschließend wurde jeder Sinter-

J. Peng (✉)
Graduate School of Science and Engineering,
Kansai University,
3-3-35 Yamate-cho, Suita, Osaka 564-8680, Japan
k666853@kansai-u.ac.jp

körper einer DCPN-Behandlung bei 673 K für 15 h bei einem Gasdruck von 200 Pa unter 75 % N₂–25 % H₂ unterzogen. Während des Plasmanitrierens wurde ein austenitisches Edelstahlsieb als Hilfskathode installiert, um eine gleichmäßige Erwärmung und eine hohe Stickstoffzufuhr zu gewährleisten. Darüber hinaus wurde jede nitrierte Probe durch Röntgenbeugung (XRD), Beobachtungen der Mikrostruktur im Querschnitt, Beobachtungen der Oberflächenmorphologie, Härteprüfungen nach Vickers, optische Emissionsspektroskopie bei Glimmentladung (GD-OES), Korrosionsprüfungen und Verschleißprüfungen charakterisiert. Die XRD- und GD-OES-Ergebnisse zeigten, dass die N-Konzentration auf der Oberfläche mit der Dauer des Kugelmahlens abnahm. Die Härteprüfung nach Vickers ergab, dass die Oberflächenhärte mit der Dauer des KugelfräSENS zunahm. Die Ergebnisse der Elektronenmikroanalyse und der Rasterelektronenmikroskopie zeigten, dass sich die abgeschiedenen und nitrierten Schichten auf den Oberflächen aller plasmanitrierten Proben trennten. Die Verschleißtests zeigten, dass die Breite und Tiefe der Verschleißspuren mit zunehmender Dauer des KugelfräSENS abnahm und die Proben somit eine erhöhte Verschleißfestigkeit aufwiesen.

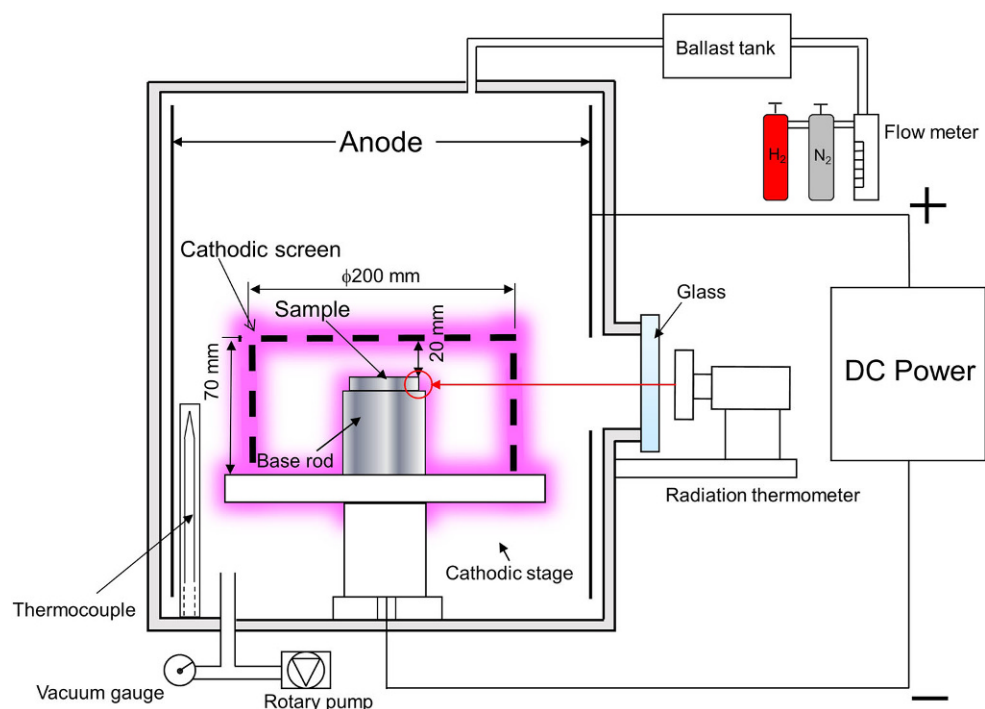
Schlüsselwörter: Hochentropie Legierung, Plasmanitrieren, KugelfräSEN, Nitrierschicht, Funkenplasmasintern, Oberflächenmodifikation

1. Introduction

Recently, many types of high-entropy alloys (HEAs) have been developed, and HEAs are known to consist of five or more metallic elements. Moreover, the compositions of the alloying elements are in the range of 5–35 at%, form-

ing a single-phase solid solution [1, 2]. Cantor *et al.* [2] produced the first HEA a CoCrFeMnNi face-centered cubic (fcc) single-phase alloy. CoCrFeMnNi has been reported to have excellent thermodynamic stability, ductility, and good tensile strength at low temperatures [3–6]; however, its hardness is approximately 160 HV [7], and the hardness of the samples prepared by other methods is approximately 130–330 HV [8–10], which are lower than that of general steel materials. Improving the hardness of soft HEAs is extremely important, and one method is the surface treatment of an alloy followed by hardening. Among various surface treatments, plasma nitriding has the advantages of short-time processing, energy saving, and environmental friendliness, and research on this topic is progressing [11–21]. Surface treatment of HEAs may increase their hardness and improve their wear resistance [22–26]. An HEA is typically produced by arc melting or casting; however, recently, anomalous microstructures and eutectic structures have been obtained by these methods [27–30]. In the spark plasma sintering (SPS) [31–34] method, a graphite die is filled with an HEA powder in a vacuum chamber and uniaxially pressurized. Simultaneously, a high pulse current is applied, and a high-temperature plasma energy is used to promote the reaction and obtain a uniform structure. In addition, a study found that a high dislocation density was observed in the deformed shear region on the powder surface, dislocations were introduced on the surface of a CoCrFeMn alloy powder by ball milling, and a simultaneous improvement in the strength of the sintered body and strain hardening occurred [34]. The introduction of such dislocations can increase the amount of nitrogen that penetrates and diffuses during plasma nitriding. Another study revealed that an expanded fcc structure formed on the surface of Cantor alloy during plasma nitriding at 673 K [20,

Fig. 1: Schematic of the setup for plasma nitriding



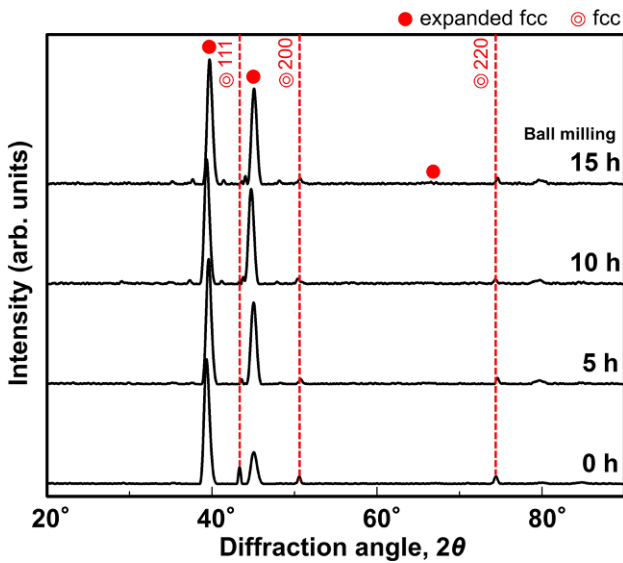


Fig. 2: XRD patterns of plasma-nitrided HEAs for ball milling times ranging from 0 to 15 h

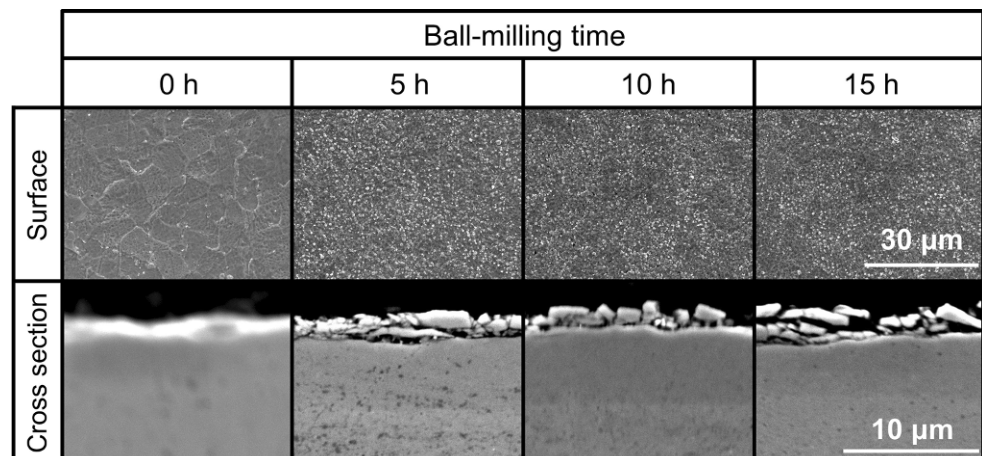
33]. In recent years, little has been reported on the surface modification of single-phase fcc CoCrFeMnNi HEA [20, 33, 35]. In the present study, after ball milling a CoCrFeMnNi gas-atomized powder, a sintered body was prepared by the SPS method followed by plasma nitriding, and the characteristics of the surface nitrided layer were evaluated.

2. Materials and Experimental Procedure

2.1 Materials

A CoCrFeMnNi alloy powder prepared by gas atomization (Sanyo Special Steel Co., Ltd., Hyogo, Japan) was used as the starting material and divided into 53–150 μm sizes by sieving. After weighing, the gas-atomized powder was taken in a container, to which 75 mL heptane was added as the solvent. Subsequently, the container was sealed, and its inside was filled with an argon (Ar) atmosphere after evacuation to prevent the oxidation of the powder during

Fig. 3: Surface and cross-sectional SEM images of plasma-nitrided HEAs for ball milling times ranging from 0 to 15 h



ball milling. Following this, the container was placed in a planetary ball mill device (Pulverisette 6, Fritsch Japan Co., Ltd.). The balancer scale was adjusted to the total weight of the balls, sample, and container before initiating the comminution. In this method, the ball milling time was varied between 0 and 15 h, the revolution was 300 rpm, and the ball to powder weight ratio was 10:1.

2.2 Spark Plasma Sintering

A ball-milled alloyed powder sample was placed in a graphite die ($\varphi 20\text{ mm}$), into which a graphite punch was subsequently inserted. The powder was sintered using an SPS apparatus (SPS-1020, FUJI ELECTRONIC INDUSTRIAL Co., Ltd., Tokyo, Japan) at a pressure of 50 MPa and a vacuum pressure of 10^{-2} Pa by passing a high pulse current. Sintering was performed at a heating rate of 80 Kmin^{-1} and at a sintering temperature of 1073 K for 10 min. When the sintering process was completed, the sample was cooled in the furnace. After sintering, the sample surface was ground to #2000 using a wet emery paper, polished using an Al_2O_3 powder (1.0 μm in diameter), ultrasonically degreased, and dried in air. Finally, the preconditioned sample was placed in a nitriding furnace for further nitriding treatment.

2.3 Plasma Nitriding

Nitriding was conducted in a plasma nitriding device (JIN-1S, NDK Inc., Kanagawa, Japan). Figure 1 shows a schematic of the plasma nitriding process. An auxiliary screen and a sample were placed on the cathodic sample stage of the device. Consequently, plasma was formed on both the sample and the auxiliary cathode screen. An auxiliary screen increases the supply of active species, such as N^+ , N_2^+ , and H^+ and increases the amount of nitrogen by penetration and diffusion. In addition, it suppresses the edge effect and allows the sample surface to be uniformly heated. [36–39]. In this study, the auxiliary screen material was an expanded mesh of SUS316L stainless-steel with 38% open area, a diameter of 200 mm, and a height of 70 mm. The distance between the sample and the screen

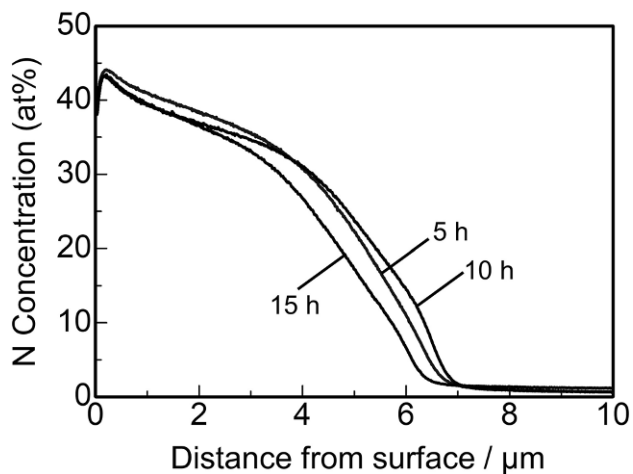


Fig. 4: GD-OES nitrogen profiles of plasma-nitrided HEAs for ball milling times ranging from 5 to 15 h

was 20 mm. After the chamber was evacuated to approximately 15 Pa, N_2 and H_2 flowed into the chamber and a direct current (DC) voltage was applied. Plasma nitriding was conducted for 15 h at 673 K under a 75% N_2 –25% H_2 atmosphere with a pressure of 200 Pa. After nitriding was completed, the sample was cooled in the furnace.

2.4 Characterization

The phase structure of each nitrided sample surfaces was characterized by X-ray diffraction (XRD; RINT-2550V, RIGAKU, Tokyo, Japan). The X-ray diffractometer was equipped with a Cu-K α radiation source operated at 40.0 kV and 300 mA, and a sample was scanned at 40.0° min⁻¹. The microstructures and compositions of all treated samples were analyzed by scanning electron microscopy (SEM; JSM-6060LV, JEOL, Tokyo, Japan), field emission SEM (JSM-6330FII, JEOL, Tokyo, Japan), electron-probe microanalysis (EPMA; JXA-8230, JEOL, Tokyo, Japan), and glow-discharge optical-emission spectroscopy (GD-OES; GD-profiler2, Horiba, Kyoto, Japan). The relative density of a sintered sample was measured using the Archimedes method. The surface hardness was measured under a load of 0.1 N using a Vickers microhardness tester (PMT-X7A, Matsuzawa, Akita, Japan). Five indentations were made on each sample, and a three-point average value (excluding the maximum and minimum values) was taken as the hardness. Wear tests were conducted at room temperature using a ball-on-disk tribometer (Anton-Paar, Peseux, Switzerland). The conditions for the wear testing were as follows: running a distance of up to 300 m, wear load of 2 N, rotation speed of 100 rpm, wear radius of 3 mm, and a diameter of 6.35 mm for the Al_2O_3 ball used as the counter material. Cross-sectional profiles of the wear tracks were measured using a surf-corder (SE300, Kosaka Laboratory, Tokyo, Japan). Pitting corrosion tests were conducted using a potentiostat. DC polarization was performed potentiodynamically from -1.0 to +1.5 V_{Ag/AgCl}, and anodic

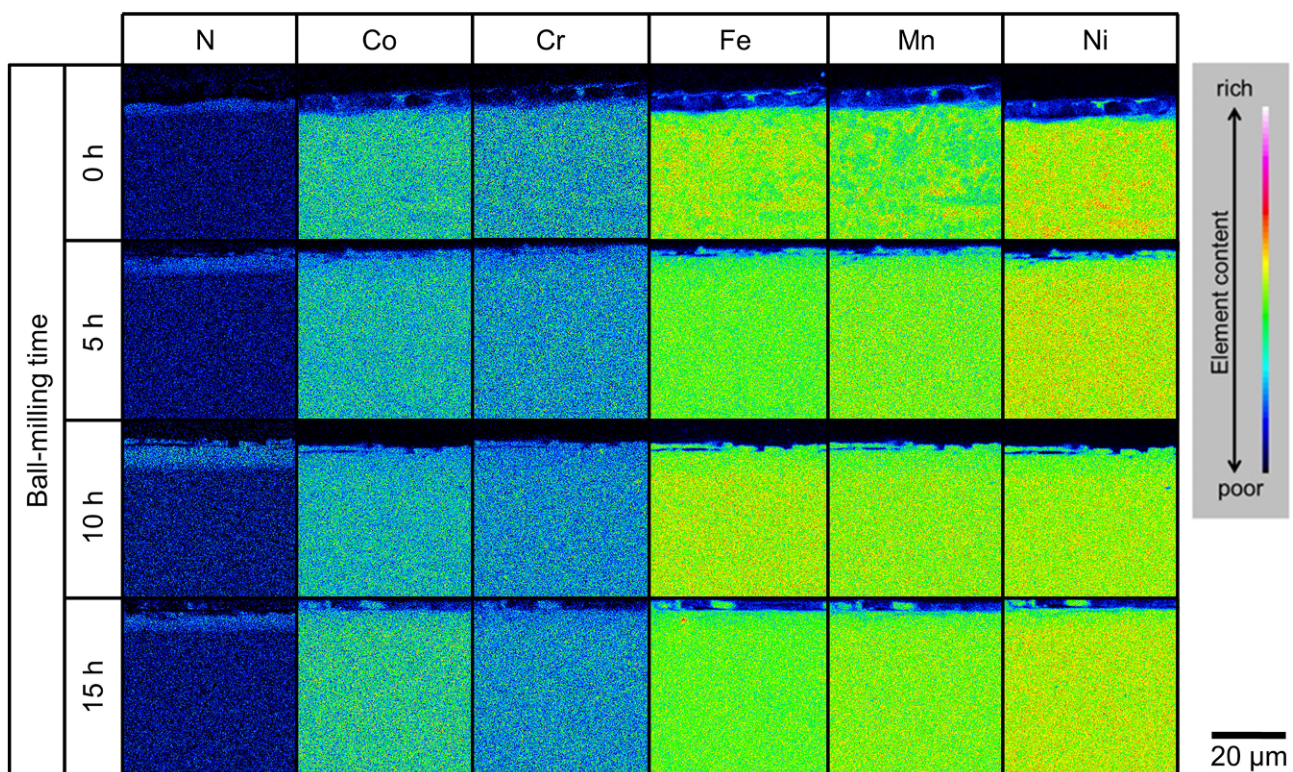


Fig. 5: EPMA element mapping images for the N, Co, Cr, Fe, Mn, and Ni of the plasma-nitrided HEA for ball milling times ranging from 0 to 15 h

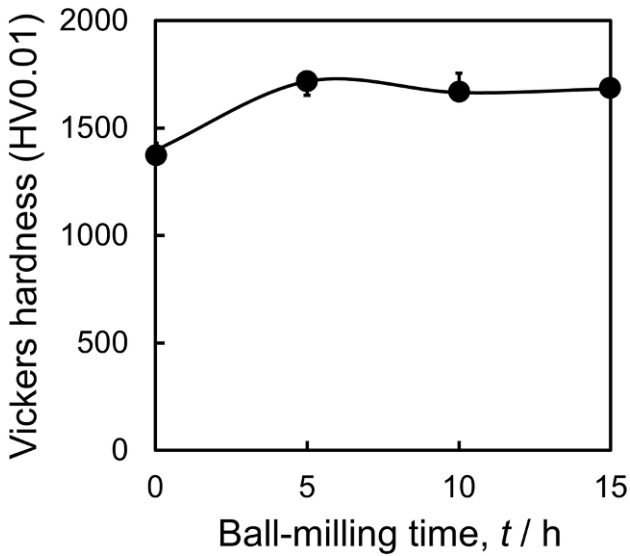


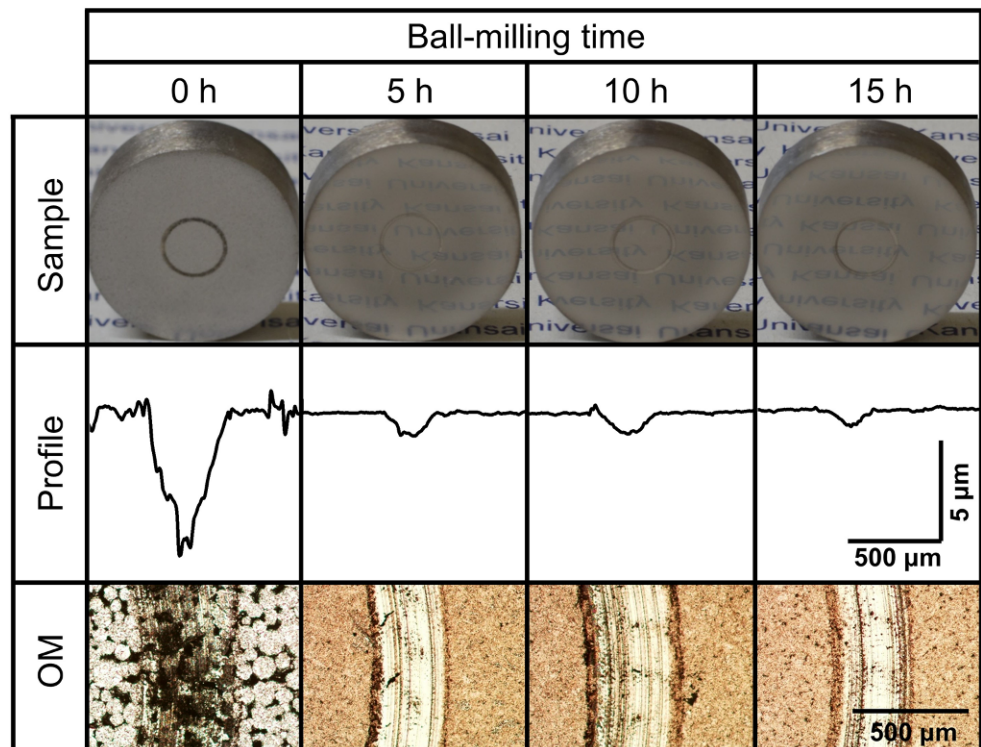
Fig. 6: Surface hardness of the plasma-nitrided HEA for ball milling times ranging from 0 to 15 h

polarization curves were recorded at a sweep speed of 1.6mVs^{-1} . Based on these polarization curves, the potential corresponding to a current density of 10Am^{-2} was selected as the pitting potential.

3. Results and Discussion

Figure 2 shows the XRD patterns of the nitrided layers of the sintered bodies formed from powders after ball milling for different times. For the times ranging from 0 to 15 h, all

Fig. 7: Appearance and wear track profile of plasma-nitrided HEAs for ball milling times ranging from 0 to 15 h after wear test



plasma-nitrided HEAs show an fcc phase and an expanded fcc structure. The obtained patterns support an expanded fcc phase with a supersaturated N solid solution with an fcc structure [20, 33]. Moreover, the formation of the expanded fcc is unrelated to the ball milling time, and it is formed when the nitriding temperature is 673 K.

The surface morphologies and the microstructures of the cross-sections of all HEA samples after plasma nitriding are shown in Fig. 3. Grain boundaries are noticeable in the 0h sample with no visible deposits. On the other hand, more deposits can be seen on the surfaces of the plasma-nitrided samples in times ranging from 5 to 15 h. A nitrided layer is not apparent from the cross-section of the 0h sample. However, the nitrided layers and deposits are noticeable in the cross-sections of the samples in the times ranging from 5 to 15 h. A dense deposited layer seems to be formed on the nitrided layer of 10-h sample.

Figure 4 shows the GD-OES nitrogen profiles of the plasma-nitrided HEAs for ball milling times ranging from 5 to 15 h. At 0h, many pores were observed on the sample surface, and GD-OES could not be obtained. High concentration of nitrogen was noticed on the surfaces of the 5, 10, and 15 h plasma-nitrided samples, and as the depth from the surface increased, the amount of nitrogen that could penetrate and solidify decreased. The thickness of the nitrided layers of the 15h, 10h, and 5h samples were $6.3\mu\text{m}$, $7\mu\text{m}$, and $7\mu\text{m}$, respectively. In terms of area, the amount of nitrogen that could infiltrate and dissolve was the highest in the 10h plasma-nitrided sample.

Figure 5 shows the cross-sectional EPMA elemental mapping images of the N, Co, Cr, Fe, Mn, and Ni in the plasma-nitrided HEAs for ball milling times ranging from 0 to 15 h. The distributions of the alloying elements are

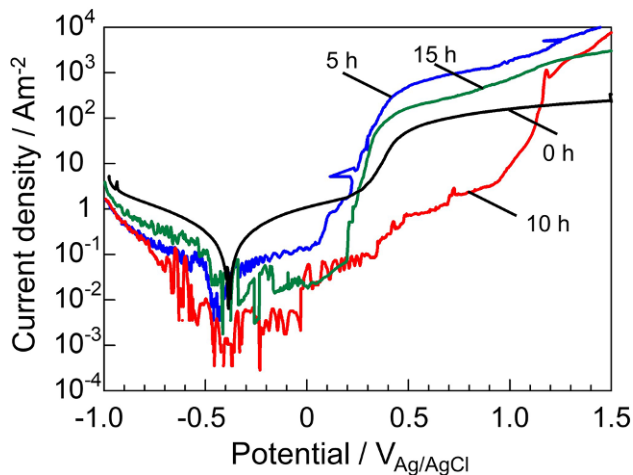


Fig. 8: Polarization curves in the 3.5 mass% NaCl of plasma-nitrided HEAs

TABLE 1 Pitting potential of plasma-nitrided HEAs for ball milling times ranging from 0 to 15 h	
Ball milling time, t/h	Pitting potential, $E_{pit}/V_{Ag/AgCl}$
0	+0.3700
5	+0.2570
10	+1.009
15	+0.2930

nonuniform in the 0 h sample, whereas they are uniformly distributed in all ball-milled samples. From the perspective of nitrogen mapping, the deposited and nitrided layers are separated on the surfaces of all plasma-nitrided samples. The thicknesses of the nitrided and deposited layers decrease in the orders of 10, 5, 15, and 0 h and 0, 15, 5, and 10 h, respectively. The thicknesses of the nitrided layers of the sample of 10 h, 5 h, 15 h, and 0 h samples are approximately 6 μm , 5 μm , 5 μm , and 3 μm , respectively.

Figure 6 shows the surface hardness values of the plasma-nitrided HEAs for ball milling times of 0–15 h. The Vickers hardness values of the samples without and with ball milling are approximately 1400 HV and exceed 1650 HV, respectively. The hardness increases in the order of 0, 10, 15, and 5 h.

Figure 7 shows the ball-on-disk wear test results of the plasma-nitrided HEAs for ball milling times of 0–15 h. The widths and depths of the sample wear marks of the ball-milled samples are significantly reduced compared to those of the sample without ball milling. The widths and depths of the wear marks and the volume of wear decrease in the order of 0, 10, 5, and 15 h.

Figure 8 shows the polarization curves in the 3.5 mass% NaCl solution of the plasma-nitrided HEAs for ball milling times of 0–15 h. Based on the polarization curves, the potential corresponding to a current density of 10Am^{-2} was selected as the pitting potential. The results of the pitting corrosion tests of the plasma-nitrided samples using a corrosive aqueous 3.5 mass% NaCl solution are summarized in Table 1. The pitting potential of a ball milling sample increases in the order of 5, 15, 0, and 10 h, and the corrosion

resistance of the plasma-nitrided HEA for ball milling time of 10 h is improved.

4. Discussion

The XRD patterns (Fig. 2) support an expanded fcc phase with a supersaturated N solid solution with an fcc structure. Moreover, the formation of the expanded fcc is unrelated to the ball milling time, and it is formed when the nitriding temperature is 673 K. By ball milling, the gas-atomized powder is solidified and shaped, and dislocations are introduced on its surface. Introducing more dislocations can dissolve nitrogen, and the thickness of the nitrided layer can be increased. Therefore, the nitrided layer of a sample after ball milling becomes thicker, and a large amount of deposit is formed on the surface. After solidification shaping, the particle size of the gas-atomized powder remains almost unchanged and the elemental distributions become uniform. The ball milling time is considered to be extremely long, and the introduced dislocations prevent the penetration and diffusion of nitrogen; consequently, the thickness of the nitrided layer is small. Compared to the previous CoCrFeMnNi S-DCPN results [20, 33], a deposited layer was observed in the ball milling samples this time. The surface hardness with ball milling is approximately 300 HV higher than the previous result [20, 33]. The denser and thicker deposited layer is believed as the cause of the improvement in the surface hardness. From the results of the pitting potential provided in Table 1, the dense deposited layer and the increase in the nitrided layer thickness are considered responsible for the corrosion resistance increase. The formation of a dense deposited layer is believed to reduce the contact area with the balls, and the wear marks suggest that a thicker and denser deposited layer improves the wear resistance, as shown in Fig. 7. According to the results of GD-OES, the nitrogen concentration of 43 at% on the top surface of the sample with ball milling was higher than the previous results of 38–41 at% nitrogen [20, 33].

5. Conclusions

Ball milling of a gas-atomized CoCrFeMnNi alloy powder was conducted to investigate its effect on the microstructure, surface hardness, wear resistance, and corrosion properties of the nitrided layer. At 673 K, the HEA was nitrided, an expanded fcc structure was formed, and the thickness of the nitrided layer was 5–7 μm . The surface hardness of the sample without ball milling was approximately 1400 HV, whereas that of a sample with ball milling improved to 1650 HV or more. Ball-on-disk wear tests showed that ball milling significantly improved the wear resistance of each sample. Finally, the pitting corrosion resistance of a 10-h ball-milled sintered sample was found to be significantly improved compared to that of sintered sample without ball milling.

Acknowledgements. This study was supported by JSPS KAKENHI Grant Number JP21K04723.

References

- Weh, J.W., Chen, S.K., Lin, S.J., Gan, J.Y., Chin, T.S., Shun, T.T., Tsau, C.H., Chang, S.Y.: Nanostructured high-entropy alloys with multiple principal elements: novel alloy design concepts and outcomes. *Adv. Eng. Mater.* **6**, 299–303 (2004)
- Cantor, B., Chang, I.T.H., Knight, P., Vincent, A.J.B.: Microstructural development in equiatomic multicomponent alloys. *Mater. Sci. Eng. A* **375–377**, 213–218 (2004)
- Gludovatz, B., Hohenwarter, A., Catoor, D., Chang, E.H., George, E.P., Ritchie, R.O.: A fracture-resistant high-entropy alloy for cryogenic applications. *Science* **345**, 1153–1158 (2014)
- Ma, D., Grabowski, B., Körmann, F., Neugebauer, J., Raabe, D.: Ab initio thermodynamics of the CoCrFeMnNi high entropy alloy: Importance of entropy contributions beyond the configurational one. *Acta Mater.* **100**, 90–97 (2015)
- Okamoto, N.L., Fujimoto, S., Kambara, Y., Kawamura, M., Chen, Z.M.T., Matsunoshita, H., Tanaka, K., Inui, H., George, E.P.: Size effect, critical resolved shear stress, stacking fault energy, and solid solution strengthening in the CrMnFeCoNi high-entropy alloy. *Sci. Rep.* **6**, 35863 (2016)
- Kauffmann, A., Stüber, M., Leiste, H., Ulrich, S., Schlabach, S., Szabó, D.V., Seils, S., Gorr, B., Chen, H., Seifert, H.-J., Heilmaier, M.: Combinatorial exploration of the high entropy alloy system Co-Cr-Fe-Mn-Ni. *Surf. Coat. Technol.* **325**, 174–180 (2017)
- Schuh, B., Mendez-Martin, F., Völker, B., George, E.P., Clemens, H., Pippan, R., Hohenwarter, A.: Mechanical properties, microstructure and thermal stability of a nanocrystalline CoCrFeMnNi high-entropy alloy after severe plastic deformation. *Acta Mater.* **96**, 256–268 (2015)
- Ayyagari, A., Barthelemy, C., Gwalani, B., Banerjee, R., Scharf, T.W., Mukherjee, S.: Reciprocating sliding wear behavior of high entropy alloys in dry and marine environments. *Mater. Chem. Phys.* **210**, 162–169 (2018)
- Joseph, J., Haghdadi, N., Shamlaye, K., Hodgson, P., Barnett, M., Fabijanic, D.: The sliding wear behaviour of CoCrFeMnNi and Al_xCoCrFeNi high entropy alloys at elevated temperatures. *Wear* **428–429**, 32–44 (2019)
- Xiao, J.K., Tana, H., Wua, Y.Q., Chen, J., Zhang, C.: Microstructure and wear behavior of FeCoNiCrMn high entropy alloy coating deposited by plasma spraying. *Surf. Coat. Technol.* **385**, 125430 (2020)
- Sun, Y., Bell, T.: Plasma surface engineering of low alloy steel. *Mater. Sci. Eng. A* **140**, 419–434 (1991)
- Zhao, C., Li, C.X., Dong, H., Bell, T.: Study on the active screen plasma nitriding and its nitriding mechanism. *Surf. Coat. Technol.* **201**, 2320–2325 (2006)
- Nishimoto, A., Tokuda, A., Akamatsu, K.: Effect of through cage on active screen plasma nitriding properties. *Mater. Trans.* **50**, 1169–1173 (2009)
- Dong, H.: S-phase surface engineering of Fe-Cr, Co-Cr and Ni-Cr alloys. *Int. Mater. Rev.* **55**, 65–98 (2010)
- Nishimoto, A., Bell, T.E., Bell, T.: Feasibility study of active screen plasma nitriding of titanium alloys. *Surf. Eng.* **26**, 74–79 (2010)
- Chemkhi, M., Retraint, D., Roos, A., Garnier, C., Waltz, L., Demangel, C., Proust, G.: The effect of surface mechanical attrition treatment on low temperature plasma nitriding of an austenitic stainless steel. *Surf. Coat. Technol.* **221**, 193–195 (2013)
- Li, Y., Wang, Z., Wang, L.: Surface properties of nitrided layer on AISI 316L austenitic stainless steel produced by high temperature plasma nitriding in short time. *Appl. Surf. Sci.* **298**, 243–250 (2014)
- Unal, O., Maleki, E., Varol, R.: Effect of severe shot peening and ultra-low temperature plasma nitriding on Ti-6Al-4V alloy. *Vacuum* **150**, 69–78 (2018)
- Sathish, T.: BONN technique: tribological properties predictor for plasma nitrided 316L stainless steel. *Mater. Today Proc.* **5**, 14545–14552 (2018)
- Nishimoto, A., Fukube, T., Maruyama, T.: Microstructural, mechanical, and corrosion properties of plasma-nitrided CoCrFeMnNi high-entropy alloys. *Surf. Coat. Technol.* **376**, 52–58 (2019)
- Hamashima, S., Nishimoto, A.: Thickening of S-phase and α -phase of various stainless steels treated by low temperature plasma nitriding using screen. *Mater. Trans.* **63**, 1170–1178 (2022)
- Wang, Y., Yang, Y., Yang, H., Zhang, M., Qiao, J.: Effect of nitriding on the tribological properties of Al_{1.3}CoCuFeNi₂ high-entropy alloy. *J. Alloys Compd.* **725**, 365–372 (2017)
- Wu, Y.H., Yang, H.J., Guo, R.P., Wang, X.J., Shi, X.H., Liaw, P.K., Qiao, J.W.: Tribological behavior of boronized Al_{0.1}CoCrFeNi high-entropy alloys under dry and lubricated conditions. *Wear* **460–461**, 203452 (2020)
- Cai, Z., Wang, Z., Hong, Y., Lu, B., Liu, J., Li, Y., Pu, J.: Improved tribological behavior of plasma-nitrided AlCrTiV and AlCrTiVSi high-entropy alloy films. *Tribol. Int.* **163**, 107195 (2021)
- Nam, H., Kim, J., Kim, N., Song, S., Na, Y., Kim, J., Kang, N.: Effect of grain size on carburization characteristics of the high-entropy equiatomic CoCrFeMnNi alloy. *Materials* **14**, 7199 (2021)
- Guo, X., Jin, X., Shi, X., Yang, H., Zhang, M., Qiao, J.: Tribological behavior of boronized Fe₄₀Mn₂₀Cr₂₀Ni₂₀ high-entropy alloys. *Metals* **11**, 1561 (2021)
- Guo, S., Ng, C., Liu, C.T.: Anomalous solidification microstructures in Co-free Al_xCrCuFeNi₂ high-entropy alloys. *J. Alloys Compd.* **557**, 77–81 (2013)
- Wang, C., Ji, W., Fu, Z.: Mechanical alloying and spark plasma sintering of CoCrFeNiMnAl high-entropy alloy. *Adv. Powder Technol.* **25**, 1334–1338 (2014)
- Nagase, T., Takemura, M., Matsumuro, M., Maruyama, T.: Solidification microstructure of AlCoCrFeNi_{2.1} eutectic high entropy alloy ingots. *Mater. Trans.* **59**, 255–264 (2018)
- Zhou, K., Li, J., Wu, Q., Zhang, Z., Wang, Z., Wang, J.: Remelting induced fully-equiaxed microstructures with anomalous eutectics in the additive manufactured Ni₃₂Co₃₀Cr₁₀Fe₁₀Al₁₈ eutectic high-entropy alloy. *Scr. Mater.* **201**, 113952 (2021)
- Joo, S.-H., Kato, H., Jang, M.J., Moon, J., Kim, E.B., Hong, S.-J., Kim, H.S.: Structure and properties of ultrafine-grained CoCrFeMnNi high-entropy alloys produced by mechanical alloying and spark plasma sintering. *J. Alloys Compd.* **698**, 591–604 (2017)
- Liu, X., Zhang, L., Xu, Y.: Microstructure and mechanical properties of graphene reinforced Fe₅₀Mn₃₀Co₁₀Cr₁₀ high-entropy alloy composites synthesized by MA and SPS. *Phys. A* **123**, 567 (2017)
- Karimoto, T., Nishimoto, A.: Plasma-nitriding properties of CoCrFeMnNi high-entropy alloys produced by spark plasma sintering. *Metals* **10**, 761 (2020)
- Li, G., Liu, M., Lyu, S., Nakatani, M., Zheng, R., Ma, C., Li, Q., Ameyama, K.: Simultaneously enhanced strength and strain hardening capacity in FeMnCoCr high-entropy alloy via harmonic structure design. *Scr. Mater.* **191**, 196–201 (2021)
- Nakajo, H., Nishimoto, A.: Boronizing of CoCrFeMnNi high-entropy alloys using spark plasma sintering. *J. Manuf. Mater. Process.* **6**, 29 (2022)
- Nagatsuka, K., Nishimoto, A., Akamatsu, K.: Surface hardening of duplex stainless steel by low temperature active screen plasma nitriding. *Surf. Coat. Technol.* **205**, S295–S299 (2010)
- Naeem, M., Waqas, M., Jan, I., Zaka-ul-Islam, M., Díaz-Guillén, J.C., Rehman, N.U., Shafiq, M., Zakaullah, M.: Influence of pulsed power supply parameters on active screen plasma nitriding. *Surf. Coat. Technol.* **300**, 67–77 (2016)
- Nishimoto, A., Fukube, T., Tanaka, T.: Effect of surface deposits on nitriding layer formation of active screen plasma nitriding. *Mater. Trans.* **57**, 1811–1815 (2016)
- Toshioka, N., Nishimoto, A.: Surface-modified layer formed by plasma nitriding using chromium screen. *Mater. Trans.* **61**, 1115–1121 (2020)

Publisher's Note. Springer Nature remains neutral with regard to jurisdictional claims in published maps and institutional affiliations.